International Journal of Thermophysics, Vol. 26, No. 6, November 2005 (© 2005)
DOI: 10.1007/s10765-005-8599-y

Photothermal Depth Profiling by Thermal Wave Backscattering and Genetic Algorithms[1]

R. Li Voti,[2,3] C. Sibilia,[2] and M. Bertolotti[2]

Photothermal depth profiling is usually applied to inhomogeneous materials to localize the optical inhomogeneity or retrieve the thermal effusivity depth profile by simply monitoring the photothermal signal after the pump beam excitation. In this paper the different kinds of inverse problems related to photothermal depth profiling are discussed, and the solutions given by thermal wave backscattering (TWBS) and genetic algorithms (GAs) are compared. Finally, the different performances and limits of validity on known linear profiles are compared.

KEY WORDS: inverse problems; nondestructive evaluation; photothermal techniques; thermal conductivity; thermal effusivity.

1. INTRODUCTION

Nondestructive evaluation of inhomogeneous materials by photothermal techniques has been the subject of many papers in recent years. Presently such techniques are widely used to evaluate different kinds of inhomogeneity, whether macroscopic subsurface defects in a homogeneous material [1, 2] or microscopic structural modifications that produce changes in both thermal and optical parameters [3–7].

Photothermal depth profiling is usually applied to such inhomogeneous materials and can be used to localize the optical inhomogeneity [7] or retrieve the thermal effusivity depth profile [8–11] by simply monitoring

[1] Paper presented at the Fifteenth Symposium on Thermophysical Properties, June 22–27 2003, Boulder, Colorado, U.S.A.

[2] CNISM and Dipartimento di Energetica, Università degli Studi di Roma "La Sapienza," Via Scarpa 14, 00161 Roma, Italy.

[3] To whom correspondence should be addressed. E-mail: roberto.livoti@uniromal.it

the surface temperature or any related photothermal signal after the pump beam pulse absorption.

In this paper we want to discuss two different kinds of inverse problems: heat source depth profiling (first type) [12] and effusivity depth profiling (second type) [13–16]. We want to show, for the first time, the equivalence of the two problems, and provide some mathematical tools to obtain solutions by thermal wave backscattering (TWBS) [9, 10] and genetic algorithm (GA) [17, 18] approaches. Finally, we compare the different performances and limits of validity on known linear profiles.

2. LOCALIZATION OF THE HEAT SOURCES

In this section we discuss the possibility to localize the internal heat sources induced by a pulsed laser beam, by simply looking at the surface temperature decay of the sample. This is a typical inverse problem of the first kind described by the following statements: (a) the sample's thermal properties are constant; (b) the sample's optical properties are a function of depth (i.e., z axis) only; and (c) the pump beam is defocused onto the sample so as to provide plane illumination in the xy plane, and is a Dirac pulse in time $\delta(t)$. Consequently, if one combines (b) with (c) the induced heat sources should be z-dependent only, and synchronous with the pump pulse according to the function $q(z)\delta(t)$, where $q(z)$ is the heat deposited per unit volume. The temperature rise in the material $T(z, t)$ is therefore given by the following Fourier diffusion equation in the half space $z > 0$:

$$\frac{\partial^2 T}{\partial z^2} - \frac{1}{D}\frac{\partial T}{\partial t} = -\frac{q(z)\,\delta(t)}{k} \quad (z > 0) \tag{1}$$

where k and D are the sample's thermal conductivity and diffusivity, respectively. The solution of Eq. (1) may be given by the Green function method. In fact, in the particular case of a heat source $q(z) = \delta(z - \zeta)$ placed at $z = \zeta$, the Green function solution of Eq. (1) is given by

$$G(z, \zeta, t) = \frac{1}{2e\sqrt{\pi t}} \left\{ \exp\left[-(z-\zeta)^2 / 4Dt \right] + \exp\left[-(z+\zeta)^2 / 4Dt \right] \right\} \tag{2}$$

where e is the sample's thermal effusivity. The two terms in Eq. (2) correspond to two heat sources: the real one placed at $z = \zeta$, and its image at $z = -\zeta$, which should be added to fulfil the adiabatic condition at the air/sample interface at $z = 0$. For a better understanding of the heat diffusion process, one may plot, for example, the Green function in Eq. (2) for a heat source placed at $\zeta = 0.4L$, where L is a characteristic depth. In

Fig. 1 the internal temperature distribution versus the normalized depth z/L is plotted for increasing time (from curves a to f). At an early time (see curve a), the temperature distribution is localized around the heat source at $\zeta/L = 0.4$. As the time increases, the heat diffuses in all directions (see curves b and c). After some time the diffusion reaches the surface, and the surface temperature starts increasing up to a maximum value at the time $t = \zeta^2/(2D)$ (see curve d). For later times the temperature distribution becomes spatially homogeneous, and starts decreasing with time as $1/\sqrt{t}$ (see curves e and f), due to the heat diffusion towards larger z. This phenomenon may be clearly seen even in Fig. 2 where the surface temperature is plotted as a function of the normalized time Dt/L^2 for different locations of the heat source. The curves from a to f correspond to a heat source placed deeper and deeper inside the sample ($\zeta/L = 0$, 0.2, 0.4, 0.6, 0.8, 1). Note that all curves reach their maximum at a particular normalized time delay $Dt/L^2 = 0.5\,(\zeta/L)^2$, that is, the time required for the heat to "*travel*" from the source to the surface. Finally, for later times all curves merge together, assuming the same typical $1/\sqrt{t}$ cooling behavior.

The case of a distributed heat source profile, with $q(z)$ an arbitrary function, may be anyway seen as a convolution of Dirac delta functions as $q(z) = \int_0^\infty q(\zeta)\,\delta(z-\zeta)\,d\zeta$. As a result, since Eq. (1) is a linear differential equation, the surface temperature may be written as the convolution

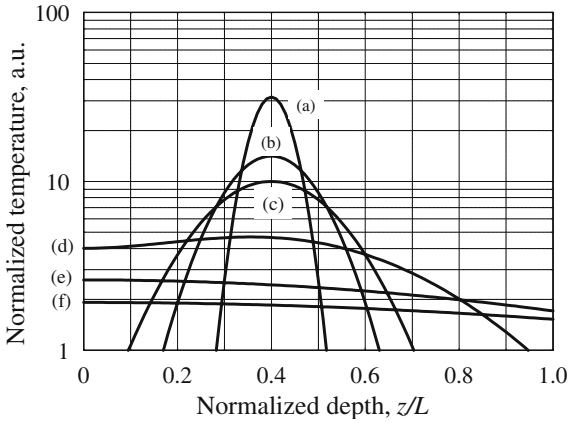

Fig. 1. Normalized temperature versus the normalized depth z/L for a single Dirac source placed at $z/L = 0.4$. Curves refer to different normalized time Dt/L^2: (a) 0.001, (b) 0.005, (c) 0.01, (d) 0.08, (e) 0.1, and (f) 1.

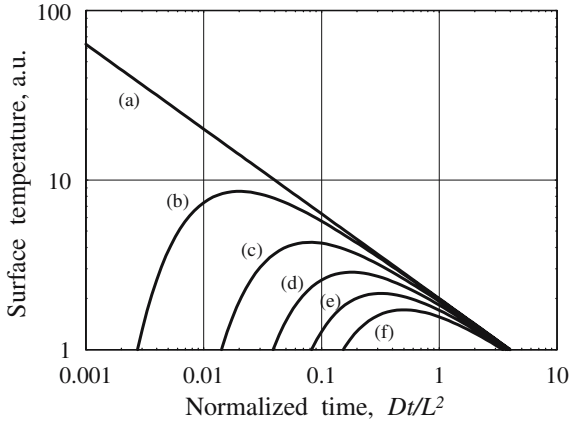

Fig. 2. Surface temperature cooling versus the normalized time Dt/L^2. Curves refer to a different location of the heat source: (a) $\zeta/L=0$, (b) $\zeta/L=0.2$, (c) $\zeta/L=0.4$, (d) $\zeta/L=0.6$, (e) $\zeta/L=0.8$, and (f) $\zeta/L=1$.

of the heat source profile by the Green function in Eq. (2) as follows:

$$T(z,t) = \int_0^\infty q(\zeta)\, G(z,\zeta,t)\, d\zeta = \frac{1}{2e\sqrt{\pi t}} \int_0^\infty q(\zeta) \left\{ \exp\left[-(z-\zeta)^2/4Dt\right] + \exp\left[-(z+\zeta)^2/4Dt\right] \right\} d\zeta \tag{3}$$

from which one easily calculates the surface temperature at $z=0$;

$$T_s(t) = \frac{1}{e\sqrt{\pi t}} \int_0^\infty q(\zeta) \exp\left[-\zeta^2/4Dt\right] d\zeta \tag{4}$$

Equation (4) shows how to calculate $T_s(t)$ once $q(z)$ is known (forward problem). The question now is: is it possible to retrieve $q(z)$ once $T_s(t)$ is measured by any photothermal technique at some time t_k, where $k \in [1, N]$? This is a typical de-convolution process (inverse problem) which may be solved by subdividing the sample into a number $M < N$ of layers of constant thickness $\Delta\zeta$. The heat source profile inside the ith layer, where $i \in [1, M]$, is kept constant at the value q_i. As a consequence, Eq. (4) is replaced by the following matrix product:

$$T_s(t_k) = T_k = \sum_{i=1}^{M} q_i \left(\int_{\zeta_i - \Delta\zeta/2}^{\zeta_i + \Delta\zeta/2} \frac{\exp\left[-\zeta_i^2/4Dt\right]}{e\sqrt{\pi t_k}} d\zeta \right) = \sum_{i=1}^{M} A_{k,i} q_i \tag{5}$$

where the matrix element $A_{k,i}$ represents the surface temperature at the time t_k generated by a constant heat source placed only in the ith layer for $z \in [\zeta_I - \Delta\zeta/2, \zeta_I + \Delta\zeta/2]$. Searching for the properties of the matrix A, one may plot the vectors $V_k = A_{k,i}$ as a function of t_k, keeping i constant, so as to obtain practically the same curves reported in Fig. 2. The clear linear independence among curves in Fig. 2, and consequently among the vectors V_k, shows that the system in Eq. (5) may be de-convoluted so as to retrieve the original vector q_i, by applying, for example, the singular value decomposition (SVD) [18]. Such a mathematical tool consists of individuating the singular values and the corresponding singular vectors associated with the kernel of the Fredholm integral equation in Eqs. (4) and (5). In Fig. 3 some singular vectors are plotted as a function of the normalized depth z/L. The curves refer to the singular vectors of order 1(◯), 2(□), 3(∇), 5(●), and 10(■) [7]. As one may see, the larger is the order, the bigger is the number of oscillations. These vectors constitute a suitable base in the space of depth profiles, so that any profile may be obtained by a unique superposition of all the singular vectors. In practice, depending on the complexity of the profile to be reconstructed, one may achieve a good accuracy even if one truncates the superposition and uses only the first N singular vectors (from order 1 to N) (truncated SVD, TSVD). As an example, we discuss the case of a hidden heat source placed in the region $0.3 \leqslant z/L \leqslant 0.7$ (see continuous line in Fig. 4). The corresponding surface temperature (see continuous line in Fig. 5) shows a peak at the normalized time $Dt/L^2 \approx 0.1$ which gives a first rough estimate of the location of the heat source at $z/L \cong 0.45$. Of course, in order to reconstruct precisely the profile, one should fit the surface temperature in the whole temporal range $Dt/L^2 \in [0.001, 10]$ by TSVD. The quality of the fit is very bad when $N = 2$ singular vectors only are used (see symbols □ in Fig. 5), but strongly improves already for $N = 5(\nabla)$. Further improvements for $N = 10(\bullet)$ or $N = 30(\blacksquare)$ are practically invisible in Fig. 5. The profiles reconstructed with the same numbers $N = 2(\square)$, $5(\nabla)$, $10(\bullet)$, and $30(\blacksquare)$ are plotted in Fig. 4. It is worth noting that the reconstruction becomes more accurate as N increases. In fact, the use of high-order singular vectors, as a result of their high spatial frequency content, generally improves the spatial resolution of the reconstruction.

A different situation happens when the surface temperature is affected by noise. Unfortunately, in this case the use of high-order singular vectors usually brings unrealistic oscillations in the reconstruction and should be avoided. In practice, there are two opposite requirements: from one side, one wants to use N as large as possible to improve the spatial resolution of the reconstruction; from the other side, the signal-to-noise ratio limits the maximum value of N in order to avoid the unrealistic profiles.

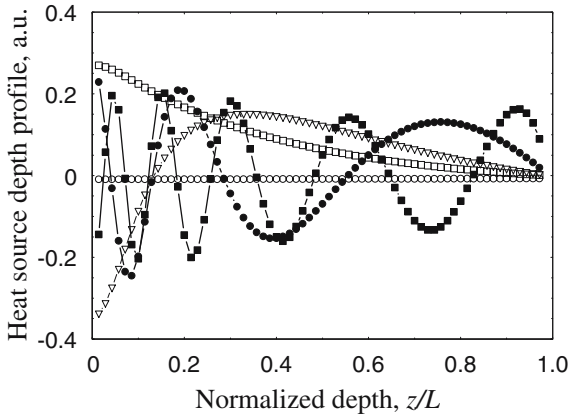

Fig. 3. Heat source profiles singular vectors of the singular value decomposition: curve (◯) $N=0$; curve (□) $N=1$; curve (▽) $N=2$; curve (●)$N=5$; and curve (■) $N=10$.

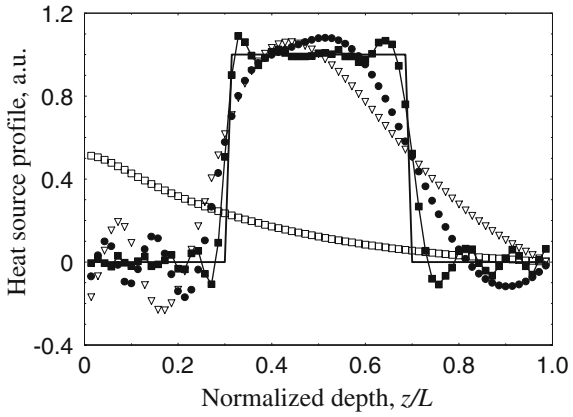

Fig. 4. Heat source versus the normalized depth z/L for a homogeneous heat source placed in the region $0.3 \leqslant z/L \leqslant 0.7$: (cont. line) original profile, (□) reconstruction with $N=2$ singular vectors; (▽) $N=5$; (●) $N=10$; and (■) $N=30$.

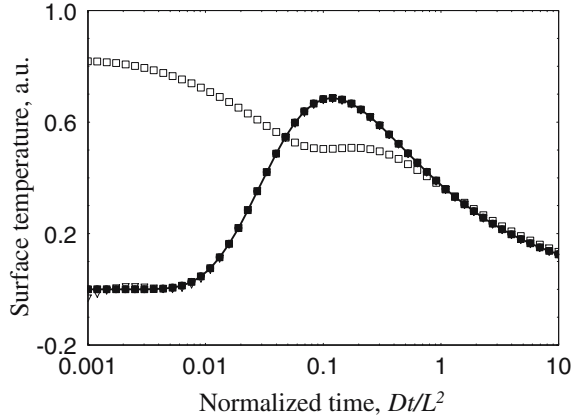

Fig. 5. Surface temperature versus the normalized time Dt/L^2 for a homogeneous heat source placed in the region $0.3 \leqslant z/L \leqslant 0.7$: (continuous line) signal to be fitted, (□) use of $N = 2$ singular vectors; (▽) $N = 5$; (●) $N = 10$; and (■) $N = 30$.

As an example in the same case studied in Figs. 4 and 5, we simply add a 10% Gaussian noise to the surface temperature (see continuous line in Fig. 6). Even in this case, the quality of the fit increases with N as shown in Fig. 6, but the same does not happen for the quality of reconstruction as shown in Fig. 7. In practice, an optimum number exists, $N_{\text{opt}} = 5$, which allows the best possible reconstruction. The way to find N_{opt} is given by the L-shape curve for residuals as shown in Fig. 8 where the norm of the surface temperature error $\|T(t) - T_{\text{rec}}(t)\| = \sqrt{\int |T(t) - T_{\text{rec}}(t)|^2 dt}$ is plotted as a function of the norm of the reconstructed profile $\|q_{\text{rec}}(z)\| = \sqrt{\int |q_{\text{rec}}(\zeta)|^2 d\zeta}$ for different values of N [18]. The optimum value $N_{\text{opt}} = 5$ is found at the knee of this L-shape curve. In fact, for $N < N_{\text{opt}}$, the error $\|T(t) - T_{\text{rec}}(t)\|$ decreases as N increases and higher-order singular vectors are used; on the other hand, for $N > N_{\text{opt}}$, the error becomes of the order of the noise and cannot decrease with N (horizontal saturation), while the reconstructed profiles exhibit large unrealistic oscillations as indicated by the large norm $\|q_{\text{rec}}(z)\|$. As a conclusion, the quality of the reconstruction depends dramatically on N_{opt} and hence on the signal-to-noise ratio. This is a general result of the information theory which fixes the limit of the reconstruction independently on the mathematical tool adopted to solve the inverse problems (TSVD, genetic algorithms, neural networks, etc.)

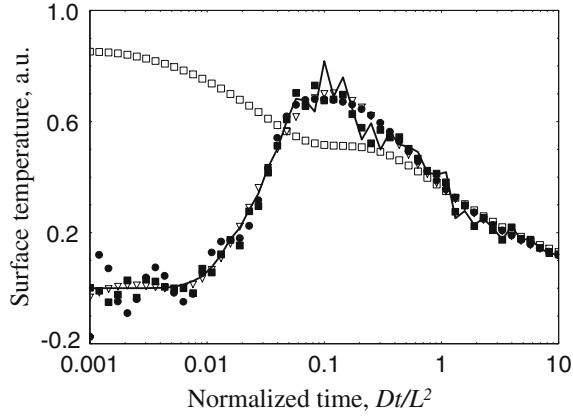

Fig. 6. Surface temperature versus the normalized time Dt/L^2 for the same heat source in Figs. 4 and 5. An additional 10% Gaussian noise has been added: (continuous line) noisy signal to be fitted, (□) $N = 2$ singular vectors; (▽) $N = 5$; (●) $N = 7$; and (■) $N = 30$.

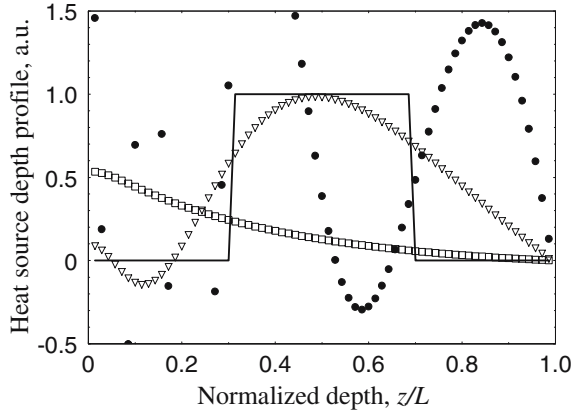

Fig. 7. Heat source versus the normalized depth z/L: (cont. line) original profile, (□) reconstruction with $N = 2$ singular vectors; (▽) $N = 5$; and (●) $N = 7$.

3. EFFUSIVITY DEPTH PROFILE

In this section we discuss the possibility to retrieve the internal thermal properties of an inhomogeneous sample by simply looking at the surface temperature cooling dynamics after the pulse heating. Such an inverse problem is classified of the second kind [12], and may be summarized as

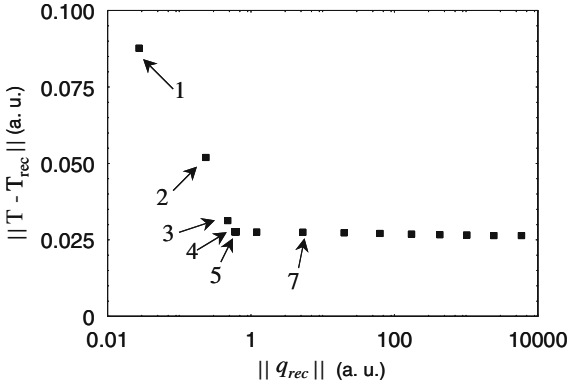

Fig. 8. L curve for residuals. The temperature error $\|T(t) - T_{\text{rec}}(t)\| = \sqrt{\int |T(t) - T_{\text{rec}}(t)|^2 dt}$ is plotted as a function of the norm of the reconstructed profile $\|q_{\text{rec}}(z)\| = \sqrt{\int |q_{\text{rec}}(\zeta)| d\zeta}$ for the first 14 singular values and singular vectors. The numbers underline the number of functions used (N). The optimum value $N_{\text{opt}} = 5$ is found at the knee of this L-shape.

follows: (a) the sample thermal properties are functions of depth (i.e., z axis) only; (b) the sample is optically opaque; (c) as in the first kind problem, the pump beam is defocused onto the sample so as to provide a plane illumination in the xy plane, and is a Dirac pulse in time $\delta(t)$. Consequently, if one combines (b) with (c), the heat is deposited at the time $t = 0$, only at the surface $z = 0$, according to the function $Q\delta(z)\delta(t)$, where Q is the heat deposited per unit area. The temperature rise in the material $T(z, t)$ is therefore given by the following Fourier inhomogeneous diffusion equation in the half space $z > 0$:

$$\frac{\partial}{\partial z}\left[k(z)\frac{\partial T}{\partial z}\right] - \rho c \frac{\partial T}{\partial t} = -Q\delta(t)\delta(z) \quad (z > 0) \tag{6}$$

where the heat capacity per unit volume (ρc) has been kept constant. Equation (6) admits exact analytical solutions just for a few classes of profiles $k(z)$. As a simple example of thermal inhomogeneity, we discuss the heat diffusion in a thin homogeneous film grown over an *infinite* thick substrate. The Laplace transform of the surface temperature is given by

$$T_{\text{s}}(s) = \frac{Q}{e_{\text{f}}\sqrt{s}}\left(\frac{1 + \text{Re}^{-2L\sqrt{s/D}}}{1 - \text{Re}^{-2L\sqrt{s/D}}}\right), \tag{7}$$

where $R = \frac{e_f - e_s}{e_f + e_s}$ is the thermal reflection coefficient defined as the effusivity mismatch between the film and the substrate, L is the film thickness, and D is the film thermal diffusivity (e_f and e_s are the thermal effusivities of the film and the substrate, respectively). The inverse Laplace transform of Eq. (7) is eventually given by Ref. 19.

$$T_s(t) = \frac{Q}{e_f\sqrt{\pi t}}\left[1 + 2\sum_{n=1}^{\infty} R^n \exp\left(-n^2\left(\frac{L^2}{Dt}\right)\right)\right] \tag{8}$$

In Fig. 9 the surface cooling is shown as a function of the normalized time Dt/L^2 for different reflection coefficients R between film and bulk. Note that when $Dt/L^2 \approx 1$ the heat diffusion reaches the rear surface and brings back the information on the thermal properties of the substrate. Obviously before that time, a regular diffusion starts in the film along the z direction (curve a, Fig. 9); since it is too early to "*feel*" the substrate, all curves merge together independently on the substrate (at any R). At a later time the heat reaches the substrate which may be less effusive ($0 < R < 1$, curves e and f), or more effusive ($-1 < R < 0$, curves b, c, and d) than the film. Generally the presence of a more (less) effusive substrate may speed up (slow down) the heat diffusion as well as the surface cooling. In the case of a very little effusive substrate (air, gases $R \approx 1$), the cooling curve stops decreasing (curve b) due to a relevant "*back diffusion*" from the substrate to the front surface, which counterbalances the main forward diffusion in the opposite direction. In the different case of a partial thermal reflection from the substrate ($|R| \neq 1$), the "*back diffusion*" is weaker than the forward diffusion; as a result, from the combination of the two heat fluxes, the surface temperature tends asymptotically to the cooling curve of the substrate with slope $-1/2$ (curves b, c, d, e, and f). In practice, in the log–log plot, there is a simple transition from the straight line $Q/\left(e_f\sqrt{\pi t}\right)$ related to an infinite thick film, to the straight line $Q/\left(e_s\sqrt{\pi t}\right)$ related to an infinite thick substrate. Therefore, from the whole surface cooling dynamics, one may retrieve information on the thermal effusivity of the substrate (i.e., the quantity R), as well as on the position of the substrate (film thickness L).

For the case of a thermal effusivity depth profile $e(z)$, the thermal conductivity $k(z) = e(z)^2/(\rho c)$, and diffusivity $D(z) = e(z)^2/(\rho c)^2$ are arbitrary functions, and Eq. (6) has no analytical solution. However, for slowly varying profiles, it is still possible to find an approximate solution very similar to Eq. (7) in the Laplace domain [10, 11, 20, 21, 25];

$$T_s(s) = \frac{Q}{e_s\sqrt{s}}\frac{1 + R(s)}{1 - R(s)} \tag{9}$$

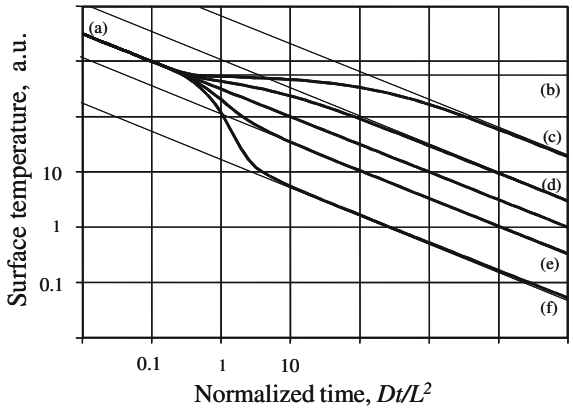

Fig. 9. Surface temperature versus normalized time Dt/L^2 for a film/bulk structure (log–log scale): curves: (a) $R=0$, (b) $R=1$, (c) $R=0.5$, (d) $R=0.2$, (e) $R=-0.2$, and (f) $R=-0.5$.

where the reflection coefficient is given by the following integral:

$$R(s)=\int_0^{\infty}\frac{-d\ln(e(z))}{2dz}\exp\left[-2\sqrt{s}\int_0^{z}\frac{d\delta}{\sqrt{D(\delta)}}\right]dz \tag{10}$$

Equation (10) has a clear physical meaning. The thermal pulse is generated by a laser at the surface, then diffuses along z, and is partially reflected back when some effusivity changes occur that act exactly as backscattering centers. The total amount of the thermal pulse reflected back is therefore given by the integral over the whole volume (dz) of all the backscattering contributions. Equation (10) is, in fact, a backscattering integral where the logarithmic term plays the role of the source for the scattering field $\left(q_{\mathrm{bs}}(\xi)=-\frac{d\ln(e(\xi))}{2d\xi}\right)$, while the exponential term represents, in the Laplace domain, the attenuation of a thermal pulse travelling two times the distance between the surface and the scattering center at the depth z (one trip to reach the inhomogeneity, plus one trip back to the surface after reflection). Note that the *thermal pulse round trip* occurs in an inhomogeneous medium, as taken into account in the diffusivity integral inside the bracket in Eq. (10). A simpler form is found if one refers to the equivalent trip of a pulse travelling in a homogeneous medium with an average diffusivity D_{av} from the surface to the equivalent depth $\xi(z)=\int_0^z\sqrt{\frac{D_{\mathrm{av}}}{D(\delta)}}d\delta$ and return. In this case, Eq. (10) becomes

$$R(s)=\int_0^{\infty}q_{\mathrm{bs}}(\xi)\exp\left[-2\xi\sqrt{s/D_{\mathrm{av}}}\right]d\xi \tag{11}$$

Finally, for the case of weak backscattering when $|R(s)| \ll 1$, Eq. (9) may be further simplified and back-transformed in the time domain as follows:

$$T_s(t) \cong \frac{Q}{e_s\sqrt{\pi t}} + 2\frac{Q}{e_s\sqrt{\pi t}} \int_0^\infty q_{bs}(\xi) \exp\left[-\xi^2/D_{av}t\right] d\xi = T_h(t) + T_{bs}(t) \tag{12}$$

where $T_h = Q\left(e_s\sqrt{\pi t}\right)$ represents the surface temperature for the case of a homogeneous sample, while T_{bs} is the backscattering contribution which contains fundamental information on the effusivity depth profile. The integrals in Eqs. (4) and (12) are very similar to each other; in fact, they both belong to the class of Fredholm integral equations of the first kind, and represent the basis of two different photothermal inverse problems. In Eq. (4) the surface temperature $T_s(t)$ is the convolution between the heat source depth profile $q(\zeta)$, and the kernel $G_1 = \exp\left\lfloor -\zeta^2/4Dt \right\rfloor$ corresponds to the diffusion process from the source at $z = \zeta$ to the surface at $z = 0$; the de-convolution of such an integral represents the solution of the first type photothermal inverse problem. Similarly in Eq. (12), the excess of surface temperature $T_s(t) - T_h(t)$ is again the convolution between the scattering depth profile $q_{bs}(\zeta)$ and the kernel $G_2 = \exp\left\lfloor -\zeta^2/D_{av}t \right\rfloor$ corresponding to the diffusion process from the surface to the scattering center at $z = \zeta$, and back to the surface; the de-convolution of such an integral represents the solution of the second type photothermal inverse problem, and allows reconstruction of the effusivity depth profile. Of course, since the second kernel is very similar to the first one, the analysis already done by TSVD for the first type problem may be simply extended to the second type problem. As an example, we report in Fig. 10 the numerical reconstruction of the thermal diffusivity of an inhomogeneous sample which changes linearly the diffusivity from D_1 to $D_2 > D_1$ within the thickness L. This linear change is well described by the reflection coefficient $R = \frac{e_1 - e_2}{e_1 + e_2} = \frac{\sqrt{D_1} - \sqrt{D_2}}{\sqrt{D_1} + \sqrt{D_2}}$ (in our case $R = -0.2$). The TSVD has been used to fit the excess of temperature in Eq. (12) in the time domain. Nevertheless, the optimum reconstruction, obtained for $N = 4$, is not fully satisfactory (see symbols $\circ$ in Fig. 10). Why? Unfortunately, Eq. (12) is an approximate formula valid only for weak backscattering $|R| \ll 1$, and not in our case ($R = -0.2$) where multiple backscattering takes place. A better reconstruction may be found by fitting directly Eqs. (9) and (10) in the Laplace domain (for positive s only), or equivalently in the Fourier domain (for imaginary $s = j\omega$). Both methods guarantee a very accurate reconstruction ($\square$ Laplace, $\diamond$ Fourier) [22]. But the differences in the L curves prove that the Fourier inversion is more stable and less sensitive to the noise. In fact,

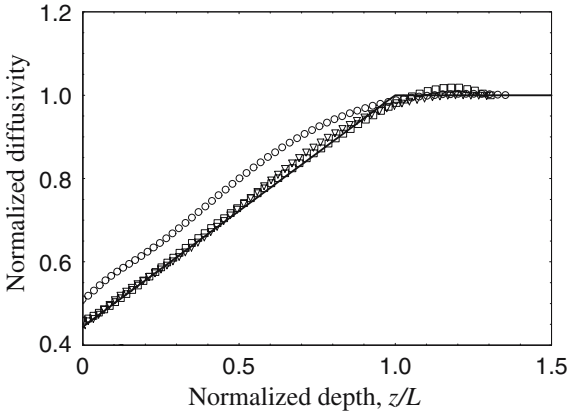

Fig. 10. Reconstruction of a linear diffusivity depth profile: (continuous line) original profile; (○) Inversion in time domain with $N_{\text{opt}} = 4$; (□) Laplace inversion with $N_{\text{opt}} = 5$; and (◇) Fourier inversion with $N_{\text{opt}} = 10$.

in the example, we use $N_{\text{opt}} = 5$ for the Laplace inversion, to be compared with $N_{\text{opt}} = 10$ for Fourier inversion.

4. GENETIC ALGORITHMS

In this section we want to apply genetic algorithms to solve, for example, the second kind problem. A GA is an artificial imitation of what happens in the natural evolution. Generally, a population of individuals evolves under the simple mechanism of the *natural selection*, trying to adapt itself to the environment [23]. In our example, a population of effusivity (or conductivity) profiles evolves trying to find the best solution of the inverse problem. How is it possible? In practice, for each profile of the population, one may calculate the cost function F defined as the temperature error $\|T(t) - T_{\text{rec}}(t)\|$ which measures how *good* is the fit with the experimental data. Depending on the cost function, the typical genetic mechanism of s*election*, *crossover*, and *mutation* may select and modify the best profiles from the old population in order to generate a better new population. The continuous application of these basic mechanisms leads to the evolution of the population towards the best solution obtained after some generations [17, 18].

As an example, we report in Fig. 11 the genetic evolution to reconstruct, from noiseless data, a thermal conductivity profile that changes linearly from $k_1 = 32\,\text{W}\cdot\text{m}^{-1}\cdot\text{K}^{-1}$ to $k_2 = 72\,\text{W}\cdot\text{m}^{-1}\cdot\text{K}^{-1}$ within the thickness $L = 0.5\,\text{mm}$ (symbols ◇). A fixed population of $M = 50$ profiles is used.

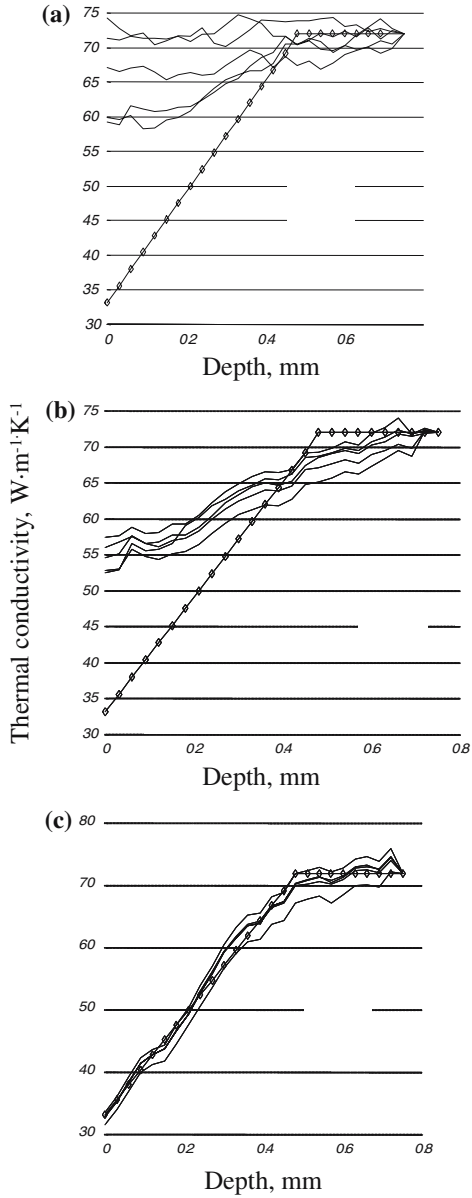

Fig. 11. Thermal conductivity reconstruction by using the genetic algorithms: (◇) original profile, (continuous lines) a few of the $M = 50$ conductivity profiles, after (a) 1 generation, (b) 10 generations, and (c) 100 generations.

Figure 11a–c refer to different moments in the evolution, respectively, after 1, 10, and 100 generations. Note that the population (continuous lines) move altogether towards the right solution (◇). This collective convergence represents the main feature of GA.

5. DISCUSSION

Finally, we want to compare the different performances and the limits of validity between the two mathematical tools introduced in this paper: TSVD and GA. In particular, we apply both methods to reconstruct thermal diffusivity profiles with different linear slopes from noiseless simulated data. In Fig. 12 the average reconstruction error for both methods, TSVD (■) and GA (●), is plotted versus the coefficient $R = \frac{e_1 - e_2}{e_1 + e_2} = \frac{\sqrt{D_1} - \sqrt{D_2}}{\sqrt{D_1} + \sqrt{D_2}}$ which is responsible for the profile slope. As one may see, the TSVD guarantees the best accuracy in the reconstruction, but only within the strict limits $-0.2 < R < 0.2$, corresponding to a slowly varying profile [24]. In fact, TSVD is applied to an approximate model of thermal wave back scattering in inhomogeneous materials (TSVD/TWBS). On the contrary, GA may be implemented on the exact heat diffusion equation and therefore may be applied to any arbitrary profile. Unfortunately, several disadvantages exist also for GA, as, for example, the complexity of the algorithm, and the slow convergence which may limit the quality of the reconstruction.

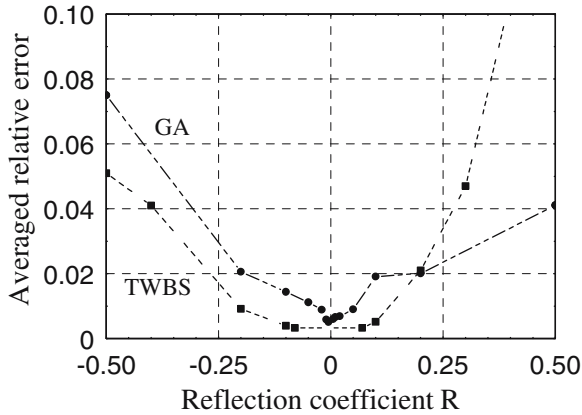

Fig. 12. Averaged profile error versus reflection coefficient R: (●) genetic algorithms; (■) truncated singular value decomposition applied to TWBS theory.

REFERENCES

1. P. M. Patel, D. P. Almond, and H. Reiter, *Appl. Phys. B* **43**:9 (1987).
2. R. L. Thomas, J. J. Pouch, W. H. Wong, L. D. Favro, P. K. Kuo, and A. Rosencwaig, *J. Appl. Phys*. **51**:1152 (1980).
3. J. Opsal and A. Rosencwaig, *J. Appl. Phys*. **53**:4240 (1982).
4. U. Seidel, T. T. N. Lan, H. G. Walther, B. Schmitz, J. Geerkens, and G. Goch, *Opt. Eng*. **36**:376 (1997).
5. T. T. N. Lan, U. Seidel, and H. G. Walther, *J. Appl. Phys.* **77**:4739 (1995).
6. S. Malkin and J. E. Ritter, *J. Eng. Indust.* **111**:167 (1989).
7. J. F. Power, *Rev. Sci. Instrum*. **72**:4067 (2002).
8. J. C. Krapez, *J. Appl. Phys*. **87**:4514 (2000).
9. C. Glorieux, R. Li Voti, J. Thoen, M. Bertolotti, and C. Sibilia, *J. Appl. Phys.* **85**:7059 (1999).
10. R. Li Voti, G. L. Liakhou, S. Paoloni, E. Scotto, C. Sibilia, and M. Bertolotti, *AIP Conf. Proc*. **463**:37 (1999).
11. X. Maldague and P. O. Moore, "Infrared and Thermal Testing,"*in Nondestructive Testing Handbook* (American Society for Nondestructive Testing, 2001), Chap. 12, p. 392.
12. J. F. Power, *AIP Conf. Proc.* **463**:1 (1999).
13. C. Glorieux and J. Thoen, *J. Appl. Phys.* **80**:6510 (1996).
14. J. Fivez and J. Thoen, *J. Appl. Phys*. **79**:2225 (1996).
15. A. Mandelis, F. Funak, and M. Munidasa, *J. Appl. Phys.* **80**:5570 (1996).
16. R. Kolarov and T. Velinov, *J. Appl. Phys.* **83**:1878 (1998).
17. R. Li Voti, C. Melchiorri, C. Sibilia, and M. Bertolotti, *Anal. Sci.* **17**:s410 (2001).
18. R. Li Voti, "Inverse Problems by Genetic Algorithms: Application to the Photothermal Depth Profiling" in *Advances in Signal Processing for Non-Destructive Evaluation of Materials,* IV Int. Workshop, X. Maldague, ed. (2002), p. 3.
19. D. L. Balageas, J. C. Krapez, and P. Cielo, *J. Appl. Phys.* **59**:348 (1986).
20. M. Bertolotti, R. Li Voti, G. L. Liakhou, S. Paoloni, and C. Sibilia, *AIP Conf. Proc.* **463**:24 (1999).
21. C. Glorieux, R. Li Voti, J. Thoen, M. Bertolotti, and C. Sibilia. *Inverse Probs.* **8** (1999)
22. J. C. Krapez and R. Li Voti, *Anal. Sci.* **17**:s417 (2001).
23. J. H. Holland, *J. Assoc. Comput. Machinery* **3**:297 (1962).
24. R. Li Voti, C. Sibilia, and M. Bertolotti, *Rev. Sci. Instrum.* **74**:372 (2003).
25. R. Li Voti, G. L. Liakhou, S. Paoloni, C. Sibilia, and M. Bertolotti, *J. Optoelectron. Adv. Mater.* **3**:779 (2001).